lubricants

MDPI

Article

Friction and Wear in Stages of Galling for Sheet Metal Forming Applications

Timothy M. Devenport [1], James M. Griffin [1], Bernard F. Rolfe [2,*] and Michael P. Pereira [2]

[1] Institute for Clean Growth and Future Mobility, Coventry University, Coventry CV1 5FB, UK; tdevenport@deakin.edu.au (T.M.D.)
[2] School of Engineering, Deakin University, Geelong, VIC 3216, Australia; michael.pereira@deakin.edu.au
* Correspondence: bernard.rolfe@deakin.edu.au

Abstract: Aluminum is a very commonly used material at present, and roughly half of the produced aluminum products undergo forming during manufacturing. Galling is a severe form of wear that occurs during sheet metal forming operations and is a common failure mode of materials in sliding contact; however, the causes and mechanisms of galling are poorly understood. In this work, sliding wear experiments were conducted to produce galling wear between a tool steel ball bearing and aluminum alloy Al5083, to study the relationship between the coefficient of friction, the lump growth on the tool and the scratch morphology. Whilst the characteristic friction regimes were observed, the characteristic damage (grooves running parallel to the scratch direction) was not observed. Instead, when galling was developed on the indenter, the scratch surface morphology displayed a series of peaks and grooves perpendicular to the scratch direction. It is likely that the difference in scratch morphology observed once galling was initiated is due to the lower hardness and reduced work hardening behavior of the Al5083 alloy, compared to the high strength steels previously examined in sheet metal forming applications. The evolution of the scratch morphology has been characterized in a novel way by investigating the distribution of the longitudinal cross-section profile height along the scratch length in relation to the three-stage friction regime observed. This showed that, as the galling wear progressed, the longitudinal cross-section profile height distribution shifts towards negative values, with a corresponding shift in the distribution of material transferred to the tool shifting to the positive. This indicates that, as the amount of material adhered to the indenter increased, the depth of the grooves on the scratch surface perpendicular to the sliding direction also increased.

Keywords: galling; wear; aluminum; steel; friction; scratch morphology; lump growth

Citation: Devenport, T.M.; Griffin, J.M.; Rolfe, B.F.; Pereira, M.P. Friction and Wear in Stages of Galling for Sheet Metal Forming Applications. *Lubricants* **2023**, *11*, 288. https://doi.org/10.3390/lubricants11070288

Received: 3 June 2023
Revised: 30 June 2023
Accepted: 30 June 2023
Published: 7 July 2023

1. Introduction

The stamping of an aluminum sheet is a common manufacturing technique used for near net shape production in several industries—such as the automotive, aerospace and consumer electronics industries and in industrial machinery—because it is cost effective, offers lightweight construction, produces little scrappage and is well suited to mass production. However, stamping along with punching and other sheet metal forming techniques is often hindered by galling wear [1–4].

Galling is a severe form of wear that occurs during sheet metal forming operations often resulting in scratches on the sheet [5], leading to significant damage to the tooling and decreased product quality. Galling failure accounts for up to 71% of the cost of die maintenance [6]. The effects of galling wear are higher energy needs, shorter tool life, lower part quality and increased cost [7]. In recent years, there has been a growing interest in understanding and mitigating the effects of galling in the sheet metal forming industry. Whilst galling is a common failure mode of materials in sliding contact, the causes and mechanisms behind it are poorly understood [8].

Galling wear is a combination of adhesive and abrasive wear, whereby material is transferred from the soft sheet to the hard tool [9], thus damaging the tool and future parts.

Hou et al. [6] explained that galling is a stochastic result of adhesive contact between two surfaces. Galling most frequently occurs between materials that have a protective oxide surface layer, such as stainless steel and aluminum [10], and so it is important to further the understanding of galling wear.

It is widely reported that galling exhibits three distinct regimes, characterized by an increase in the coefficient of friction (COF) between each regime, as shown in Figure 1. Initially, in stage 1 (before galling) the friction coefficient is low and reasonably constant, increasing sharply into stage 2 (galling initiation and transition), before increasing further and wildly fluctuating in the final stage, stage 3 (severe galling).

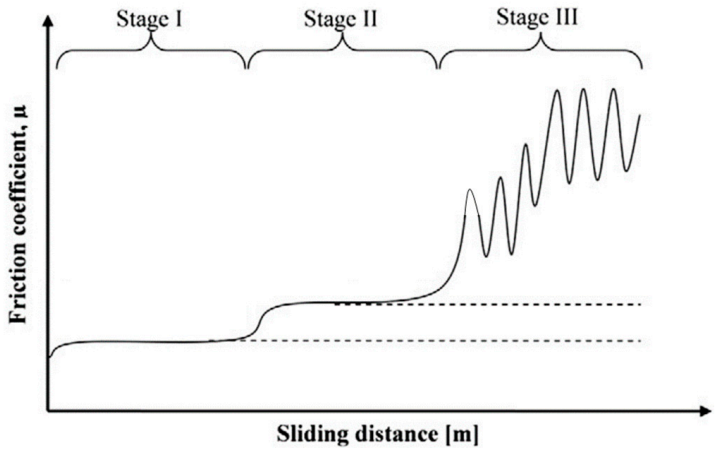

Figure 1. Typical friction curve for progressing galling wear, adapted with permission from Eriksson et al. [11].

Vilhena et al. [10] examined the galling wear of the aluminum and M2 steel tribopair and confirmed a sharp rise in the curve of the friction force vs. normal force can be used as a signal for galling initiation. Heli et al. [12] found the rapid increase in the friction coefficient, at the running-in stage under dry sliding contact conditions, was due to the formation of an aluminum transfer layer between the contact surfaces. The friction coefficient stabilized at a high value, indicating that a dynamic equilibrium was achieved between the generation and ejection of loose wear particles or the third body (as opposed to the erratic third stage).

Gaard et al. [13] describe the initial surface damage in steels occurring due to plastic deformation and the flattening of the track, with subsequent sliding and transformation into the second frictional regime occurring due to the transition in wear mechanisms to the abrasive scratching of the sheet surface. At this stage, Gaard et al. [13] report the track width was observed to be significantly wider as compared to the initial regime. Finally, further sliding leads to the second transition in friction, where scratching was found to transform into severe adhesive wear of the entire contact area. This damage is reported by other authors, such as Sindi et al. [14] as shown in Figure 2A–C. However, Sindi et al. [14] also report on the surface damage after stage 3, as shown in Figure 2D.

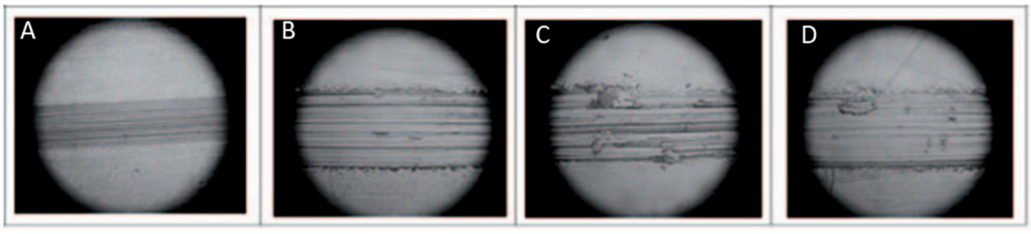

Figure 2. Sheet morphology from a slider on flat sheet tests of steel-on-steel under a 125 N load, and 630 mm/min sliding speed, reproduced with permission from Sindi et al. [14].

Sheets of the 5000-series AlMg alloys are almost exclusively used for components inside the car body, e.g., for the structural parts or for inner closure panels [15]. Therefore, studying the galling behavior of this alloy will allow for the bridging of knowledge between the well-researched tribopairs such as steel on steel and 7000-series aluminum alloys and steel wearing against even softer aluminum alloys such as the 1000, 3000 and 6000 series.

Yang et al. [16] investigated friction evolution due to lubricant breakdown in warm aluminum forming processes and showed how the damage accumulates in AA7075 during pin on disc tests, as shown in Figure 3. Initially, ploughing grooves were observed by Yang et al. [16] on the aluminum surface and the wear track was clearly visible at the low friction stage, indicating that the boundary lubrication occurred during this stage (Figure 3a). It was stated that the friction force arose from the adhesion force between the asperity contacts and the ploughing of hard asperities on the steel pin surface (as well as the effects of lubricant failure). At the beginning of the second stage (point 2), the coefficient of friction began to increase, which Yang et al. [16] attributes to aluminum wear particles agglomerating and forming wear debris lumps on the wear track, as shown by the dark areas in Figure 3b. As the lubricant failed, Yang et al. [16] reported that a significant number of asperities at the contact interface came into contact, resulting in the detachment of the aluminum wear particles and the subsequent formation of wear debris lumps on the wear track on the blank. As sliding proceeded (point 3), the area covered by wear debris lumps increased, as shown in Figure 3c. This means an increased unlubricated contact area at the interface, which would have caused an increase in the coefficient of friction. At the third stage (point 4), friction fluctuated severely at a value of approximately 1.5, which could be due to the breakdown of the lubricant leading to direct contact between the steel pin and warm (300 °C) aluminum blank [16]. As a result of the dry sliding, the strong adhesive friction force between the steel and hot aluminum with intimate contact could have contributed to the high value of coefficient of friction. Large numbers of aluminum wear particles were generated and formed wear debris lumps on the wear track, as illustrated in Figure 3d, resulting in the severe fluctuation of friction values [16].

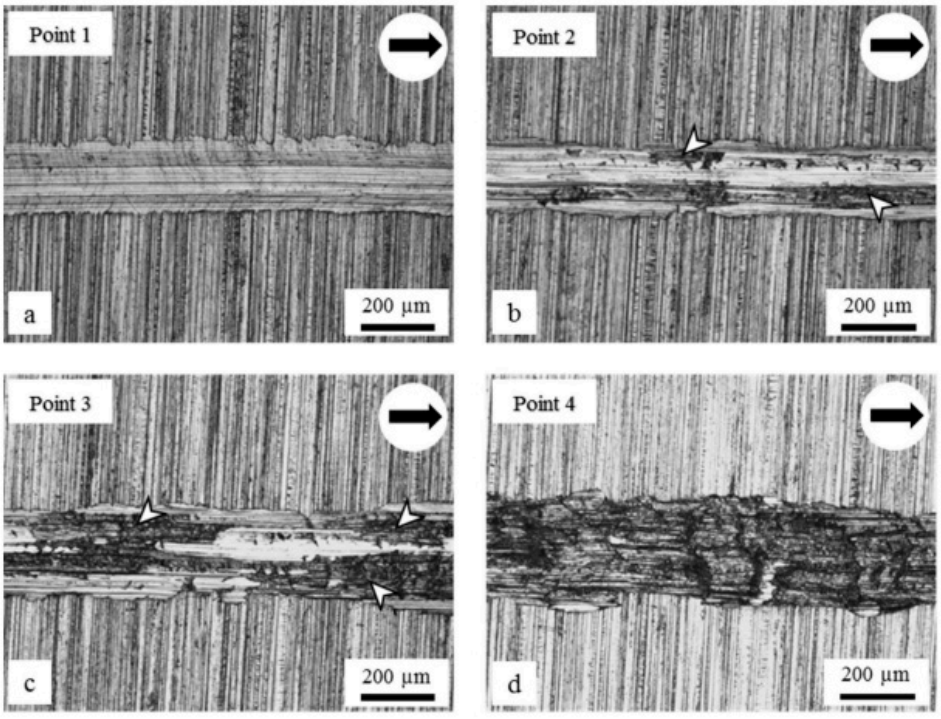

Figure 3. Optical microscopy images of the aluminium alloy wear track, showing how the damage evolves with friction (at elevated temperature of 300 °C), reproduced with permission from Yang et al. [16].

There are several disagreements/differences in the literature regarding the evolution of the worn surface morphology during galling, possibly due to the stochastic nature of galling and the fact that the micro-scale galling behavior is complex and can be sensitive to small changes in the conditions. Whilst it is widely reported that the tribological behavior of two surfaces depends strongly on the conditions of the tribosystem, conditions such as tool geometry and materials of the rubbing surfaces, atmosphere and temperature, possible lubrication and friction between the contacting surfaces, contact pressure, sliding speed all contribute to this tribosystem. Moreover, it is known that in ambient room temperature environments, contaminant films are present on metallic surfaces. The main environmental effect is the adsorption of oxygen and the oxidation of metals. It has been shown that clean metal surfaces in contact can result in severe adhesion [17,18]. Therefore, in the laboratory testing environment, it is important to examine the galling behavior for the triboconditions that are close to those experienced in the real (industrial) wear processes.

The goal of this research is to investigate the underlying mechanisms of galling wear in sheet metal cold forming by studying the galling behavior of a hard tool in sliding against an aluminum plate, under conditions not conducive to oxide production in the contact. This is achieved by conducting dry sliding wear tests between a spherical steel indenter and an Al5083 plate at room temperature, low sliding speed and low load to reduce the effects of frictional heating. The primary results examined are the evolution of the friction coefficient, lump growth on the indenter and scratch morphology. New insights into the galling behavior and methods of characterizing the scratch surface morphology and galling stages are gained.

2. Materials and Methods

Dry sliding of a spherical steel indenter on an Al5083 plate has been employed to investigate the galling wear behavior.

2.1. Materials

The indenter used was a commercially available Chrome–Molybdenum high tensile steel (AISI 4140) ball bearing, 10 mm in diameter, with a reported hardness of 207 HV [19]. The same ball bearing was reused for each scratch stroke to observe how the damage accumulated with the sliding distance. However, once galling had occurred (as identified by the coefficient of friction and microscopy, described below), a fresh indenter was used.

The plate material was an aluminum alloy, Al5083 H32 of 3 mm thickness. This is a commercially available alloy used in the automotive industry for producing lightweight car body components.

To simulate industry, both the plate and indenters were tested in the "as-received" condition. There were no additional in-house treatments for either component. The plates were wiped with acetone and left to air dry prior to testing to remove any surplus dust or contaminants. The hardness of the plates was measured to be 100 HV (corresponding to the manufacturers' reports of 89 HB), using a Struers Microhardness tester using a Vickers indenter with a 300 g load. The plate roughness measured using an Alicona InfiniteFocus optical profilometer is given in Table 1, and the chemical composition is given in Table 2.

Table 1. Sample plate roughness values (experimentally measured).

Plate	Ra (in Sliding Direction) (μm)	Ra (across Sliding Direction) (μm)
1	0.027	0.202
2	0.031	0.275
3	0.024	0.231
4	0.023	0.229
5	0.021	0.286
6	0.031	0.243
Average	0.026	0.244

Table 2. Chemical composition [20].

Element	% Present
Si	0.4
Fe	0.4
Cu	0.1
Mn	0.4–1.0
Mg	4.0–4.9
Zn	0.25
Ti	0.15
Cr	0.05–0.25
Al	Balance

2.2. Test Setup

Scratch tests were conducted using a Bruker TriboLab UMT machine, Figure 4. The Bruker UMT TriboLab can precisely measure the position of the indenter (Z height, mm) and the position of the stage. The load cell in the Bruker UMT TriboLab was used to measure the frictional forces (N) and applied load (N). Both the positions and loads were measured at a sampling rate of 1 kHz. The sample plates were attached to the Bruker stage via the four bolts shown and the indenter in the indenter holder.

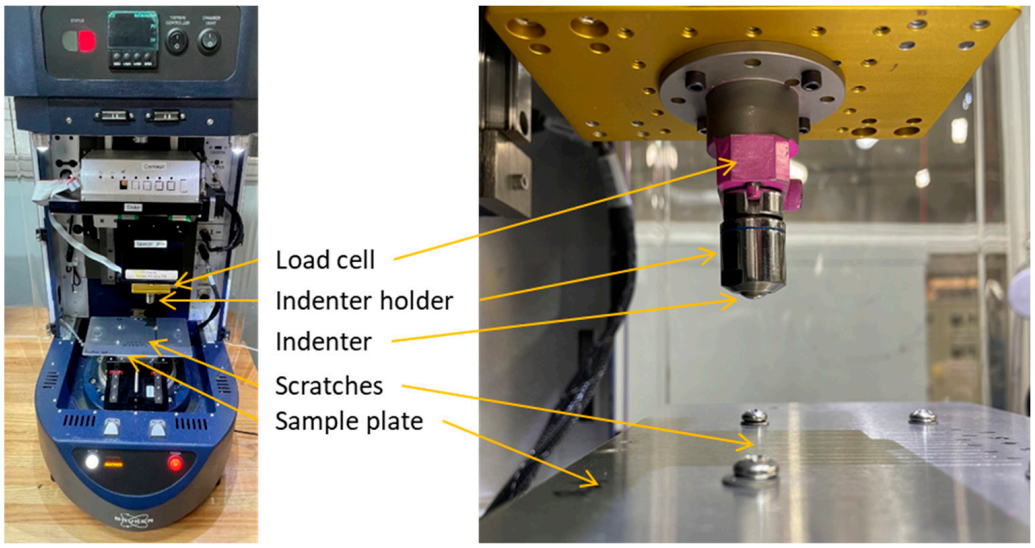

Figure 4. Bruker TriboLab UMT as used for this experimental regime.

Immediately after each scratch, the indenters were measured using an Alicona Infinite-Focus optical profilometer with no additional cleaning. The sample plates were measured later, after all scratches were conducted on the plate, also with no additional cleaning. By using optical profilometry, visual observations of the scratch morphology on the sheet material and associated material built-up edge and lump growth on the tool were conducted. The longitudinal cross-section profile of the scratch was measured within the scratch width (width of the measurement = 0.1 mm, as shown in Figure 5), and across the lump growth on the indenter. For analysis of the lump growth on the indenter, it was necessary to use the form removal tool in the Alicona software. This "flattening" of the scan surface allowed an easier comparison between the indenter surfaces, measurement of the volume of material adhered and, therefore, better understanding of the galling evolution.

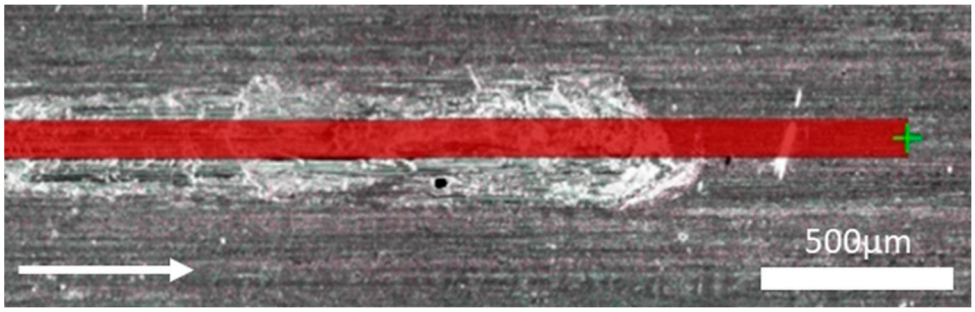

Figure 5. Example of the profile form measurement of a test that exhibited stage 3 galling. The white arrow indicates the indenter sliding direction.

2.3. Data Processing

As described above, the coefficient of friction was recorded continuously during the scratch tests. Using the friction coefficient data, the three stages of galling were differentiated using the MATLAB software package, as illustrated in Figure 6. The transition point between the end of stage 1 and the start of stage 2 was found using MATLAB software's "Ischange" function on the smoothed coefficient of the friction data. This function was used to find the point of greatest positive gradient change in the coefficient of friction, prior to the coefficient of friction exceeding 0.5, as it was assumed (based on observation of all the tests) that a coefficient of friction value of 0.5 or higher was in the middle of stage 2. The transition point at the end of stage 2 and start of stage 3 was determined by the first instance in which the coefficient of friction was greater than 0.9. Again, this rule was developed based on the analysis of all of the test data and galling observations. If this start of post galling was very close to the end of the test, i.e., after more than 95% of the test was completed, this phase was excluded, and the test characterized as only have stage 1 and stage 2. Similarly, if a transition to stage 2 happened near the end of the scratch, this test was characterized as only exhibiting stage 1.

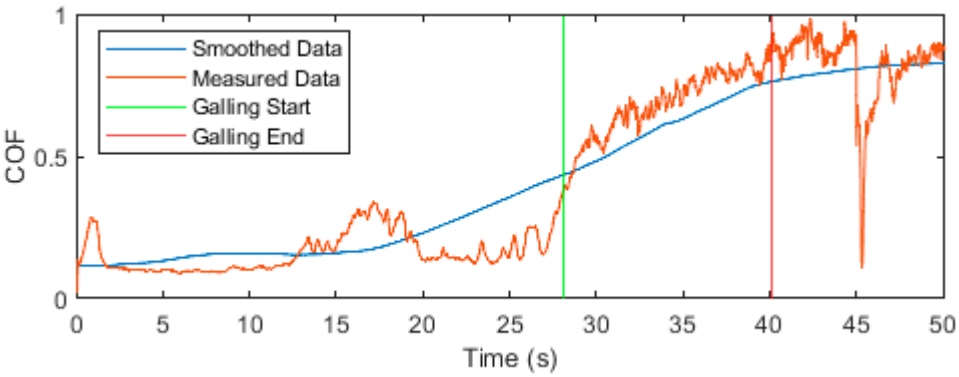

Figure 6. Example coefficient of friction curve for progressing galling wear.

2.4. Test Conditions

The scratch tests were conducted using a load control for the normal force. All scratches applied a constant 10 N normal load, using a load cell with a load range of 0.5 N to 50 N and a load resolution of ±2.5 mN. This load generates a maximum contact pressure of 650 MPa (mean contact pressure of 430 MPa), based on Hertzian contact pressure calculations assuming elastic deformation. This contact pressure closely corresponds to the contact pressures in the sheet metal forming and other works reporting on the galling of aluminum [12,21]. A total of 34 scratches were successfully performed on the sample plates. Since some tests were the result of the same ball sample continuing after the first or second 50 mm scratch length increment, these 34 scratch segments corresponded to 22 individual ball samples as shown in Table 3.

Table 3. Summary of scratch length and galling stages observed for all tests.

Ball Sample Number	Galling Stage(s) Observed for Scratch Increment A (0–50 mm)	Galling Stage(s) Observed for Scratch Increment B (50–100 mm)	Galling Stage(s) Observed for Scratch Increment C (100–150 mm)	Total Scratch Length (mm)
1	1, 2, 3	-	-	50
2	1	-	-	24
3	1	-	-	24
4	1	-	-	36
5	1, 2	-	-	50
6	1, 2, 3	-	-	50
7	1, 2, 3	-	-	50
8	1, 2, 3	-	-	50
9	1, 2, 3	-	-	50
10	1, 2, 3	-	-	50
11	1	2	3	150
12	1	2	3	150
13	1, 2	3	-	100
14	1	1,2	-	100
15	1, 2	-	-	50
16	1, 2	-	-	50
17	1, 2	3	-	100
18	1, 2	3	-	100
19	1, 2	3	-	100
20	1, 2	3	-	100
21	1, 2	3	-	100
22	1, 2	3	-	100

The sliding speed was kept to 1 mm/s to minimize the effects of frictional heating during the test (it has been reported that sliding speed affects galling wear [22]). The majority of tests were stopped after severe galling was detected; however, some tests were stopped at the moment the coefficient of friction reached 0.9, so the total scratch length for each sample varied, depending on when the galling occurred. Due to the stochastic nature of galling initiation and progression, the total sliding distance for each test varied from 24 mm up to 150 mm. The maximum scratch length that could be achieved in one length on the sample was 50 mm. Therefore, scratches longer than 50 mm consisted of more than one scratch (using the same indenter). For example, for the case of the tests with 150 mm scratch lengths, these consisted of three consecutive scratches each of a length of 50 mm. The scratch tests were conducted using a load control for the normal force. All scratches applied a constant 10 N normal load, using a load cell with a load range of 0.5 N to 50 N and a load resolution of $\pm$2.5 mN. This load generates a maximum contact pressure of 650 MPa (mean contact pressure of 430 MPa), based on Hertzian contact pressure calculations assuming elastic deformation. This contact pressure closely corresponds to the contact pressures in sheet metal forming and other works reporting on the galling of aluminum. A total of 34 scratches were successfully performed on the sample plates. Since some tests were the result of the same ball sample continuing after the first or second 50 mm scratch length increment, these 34 scratch segments corresponded to 22 individual ball samples as shown in Table 3; most scratch tests were not stopped until the end of the 50 mm scratch increment. Lubricant was not used.

3. Results

The galling wear in this manuscript has been characterized and investigated via the coefficient of friction vs. time measurements, the scratch morphology and the lump growth on the indenter.

3.1. Friction

The coefficient of friction from each experiment, categorized by the stages of galling observed, is given in Figure 7. The rest of the results are correlated against this friction measurement. It is evident that the friction did not increase when the galling did not occur (as shown by Figure 7A). Additionally, an increasing coefficient of friction can be seen in the second stage of galling. Finally, the third stage exhibits the highest coefficient of friction of approximately 1.

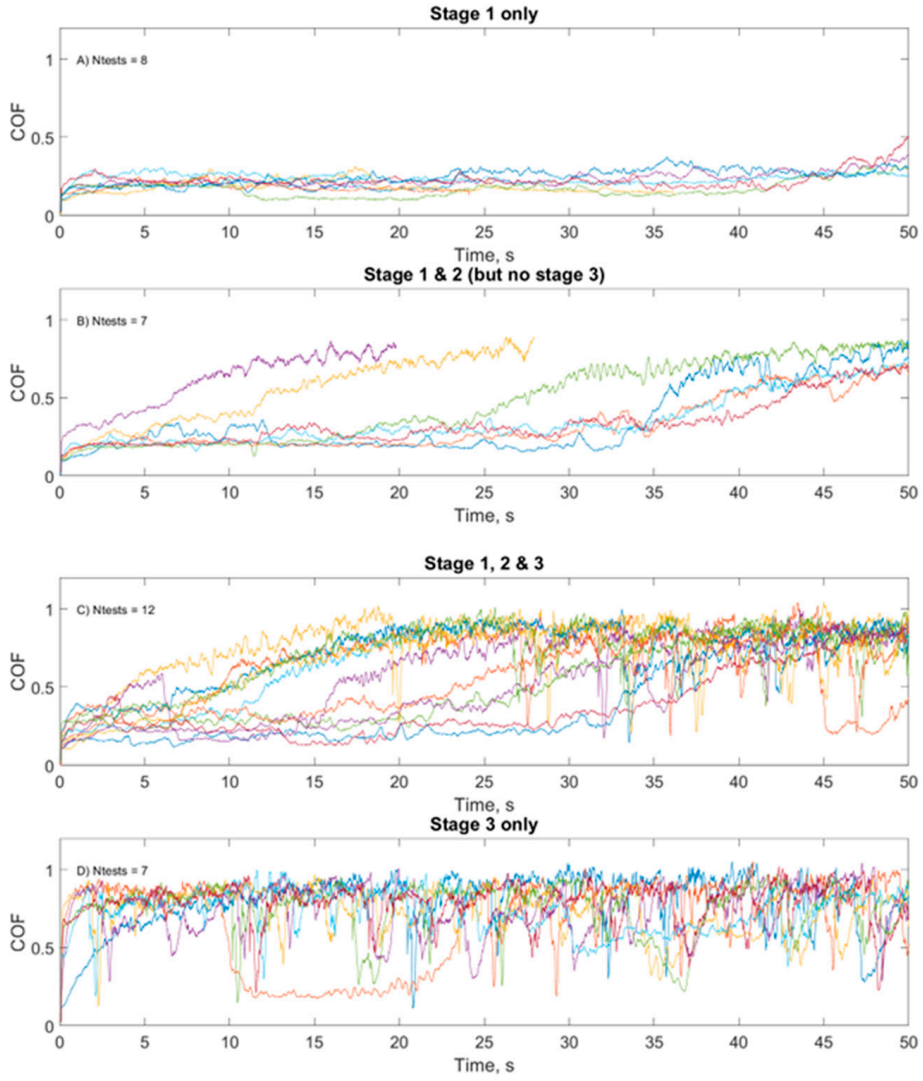

Figure 7. Coefficient of friction curves for all tests. Refer to Table 3 for reference on the tests and stages.

3.2. Lump Growth on the Tool

Figure 8 shows an example of an unworn/new indenter ball and the lump growth on the indenter after successive 50 mm scratches (up to 150 mm sliding). Figure 9 shows the measured volume of transferred material on all of the balls of the indenters. From both figures, it is evident that there is more material transferred at later stages of the galling process.

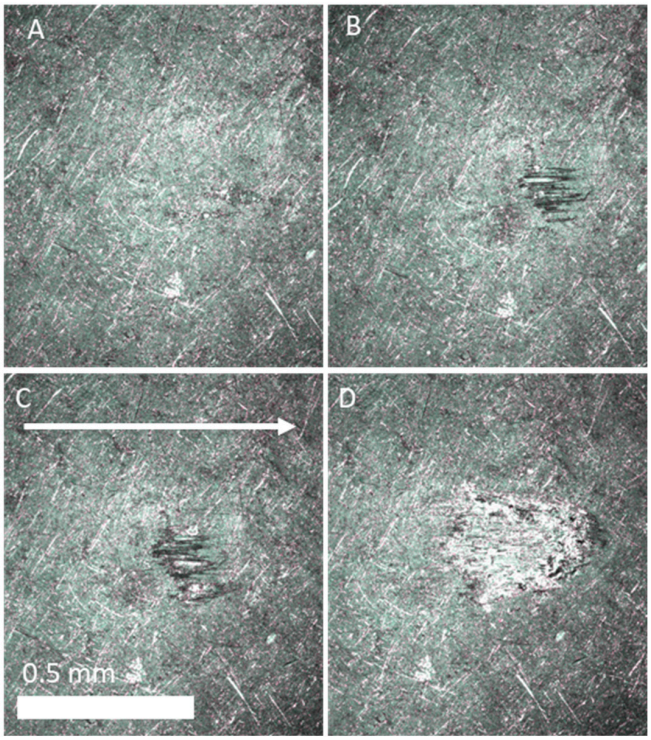

Figure 8. Lump growth on the tool. (**A**) Unworn, (**B**) 50 mm sliding, (**C**) 100 mm sliding, (**D**) 150 mm sliding. The white arrow indicates the sheet sliding direction.

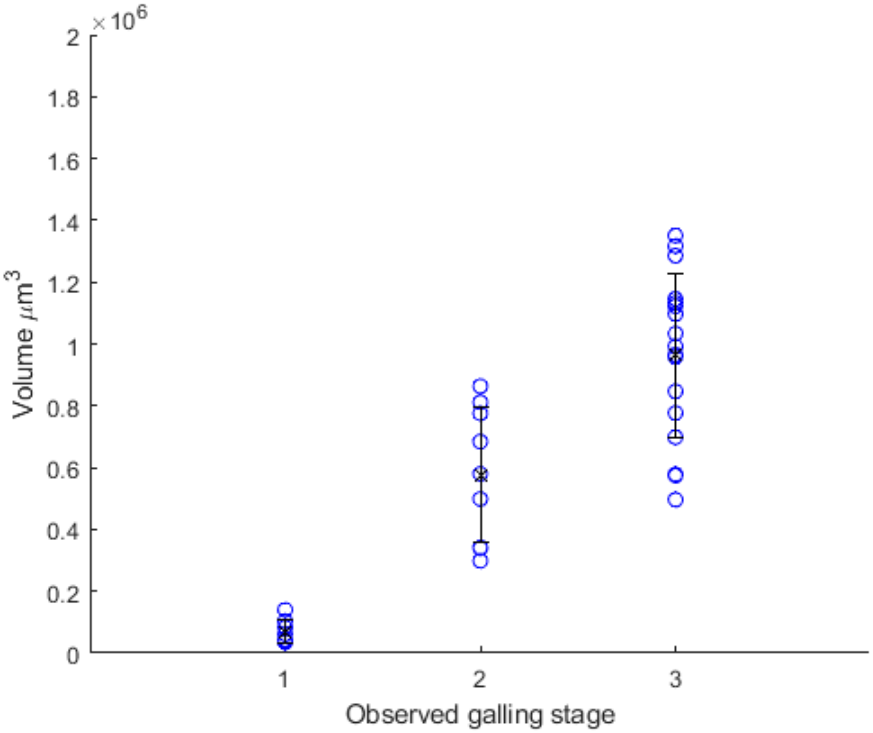

Figure 9. Lump growth—volume of material transferred to the indenter for each galling stage.

Figure 10 shows the cross-sectional shape of the build-up on the indenter between each stage. Note that the baseline surfaces on the balls in these cross-sections are flat, because the spherical indenter surfaces were "flattened out" using the Alicona software procedure described in Section 2.2. When examining the cross-sectional profiles, it is notable that there is little to no evidence of transferred material on the indenter during stage 1. However, a

very uniform lump appears for stage 2, which then typically evolves into a larger lump in stage 3. However, the lump growth on some of the indenters in stage 3 results in a very steep build up on the leading edge of the indenter.

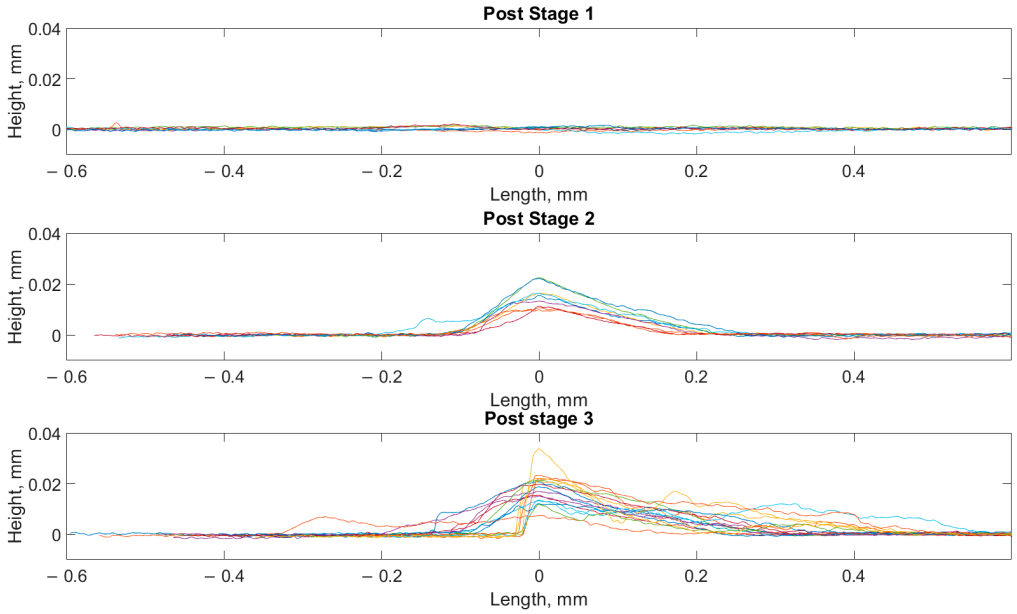

Figure 10. Cross-sections of lump growth on all of the indenters after each segment of the scratch tests, separated by the stage of galling. The sheet sliding direction is from left to right.

Figure 11 shows the distribution of the height of the build-up on the indenter, to mirror the analysis of the scratch morphology in the following section. All stages have a high number of points in and near the 0 mm profile height, as this is close to the reference plane and represents the profile height of the unworn surface. However, the number of points further away from 0 mm is indicative of material build up. In stage 1, most of the data are centered around the 0 mm profile height, with 100% of the profile height data points within $\pm$0.002 mm. However, stage 2 shows a difference compared with stage 1, where it is evident that there is material build-up in the positive area on the histogram. Stage 3 shows more of this build up, in line with the 2D profiles shown in Figures 9 and 10.

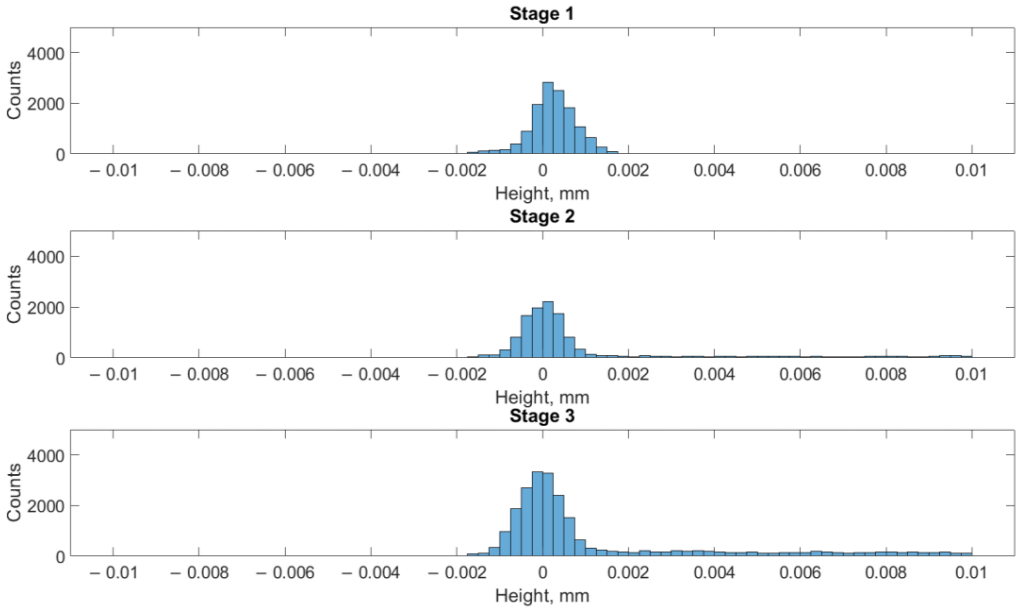

Figure 11. Distribution of the build-up on the indenter.

3.3. Scratch Morphology

Figure 12 shows the surface damage observed on the plate surfaces after the testing, as measured via the optical surface profilometer. This figure shows that there are clear differences between the scratch surface morphology for each of the galling wear stages. In particular, after stage 1, it is evident that the evolution of the surface damage is characterized by the appearance and evolution of peaks and troughs perpendicular to the scratch direction.

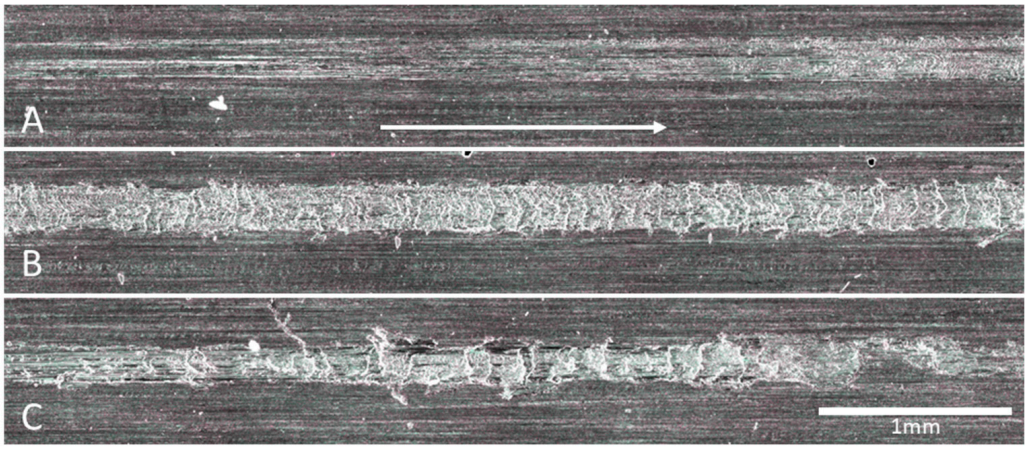

Figure 12. Magnified images of the three stages of galling wear for the different galling stages: (**A**) stage 1, (**B**) stage 2, (**C**) stage 3.

The scratch morphology for all tests is summarized by the longitudinal scratch profiles shown in Figure 13, as measured by the optical profilometer. These longitudinal profiles were obtained from the center of the scratch (as described in Section 2.2) and show the profile height along the scratch length. This figure shows a clear difference in the profile of the stage 1 scratch surface, in comparison to stage 3 scratch surface after severe galling wear. The progressive change in scratch morphology can be observed in Figure 13C, for the scratch test segments that showed all three stages of galling wear. To better observe the series of peaks and troughs in the scratch seen in the profile form measurement, a histogram of these height measurements is shown in Figure 14. In Figure 14 there is a clear change in the profile height distribution between each stage of the galling wear, with each successive stage shifting the distribution further to the negative values of profile height. This indicates that there are deeper trough-like features in the center of the scratch in stage 3, which correlates with the visual observations shown in Figure 12C.

There are noticeably more counts, an order of magnitude greater, for Figure 14 in comparison to Figure 11. This is because the length of the scratch (and therefore the measured length of the cross-sectional height) is much longer than the length of the cross-sectional height of the indenter, but the resolution of these measurements is the same. Thus, there is naturally an order of magnitude more counts for Figure 14 than Figure 11.

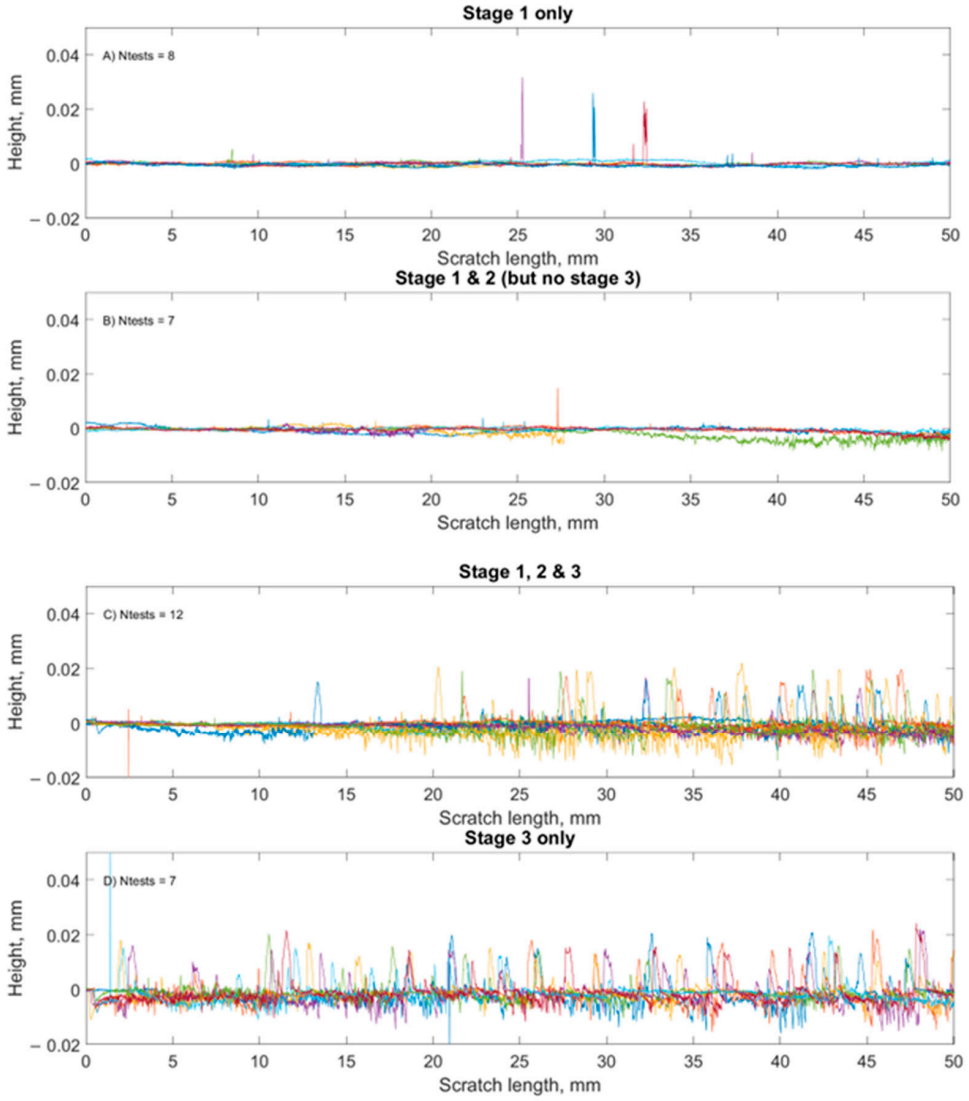

Figure 13. Evolution of the scratch morphology along the scratch length, within the scratch width.

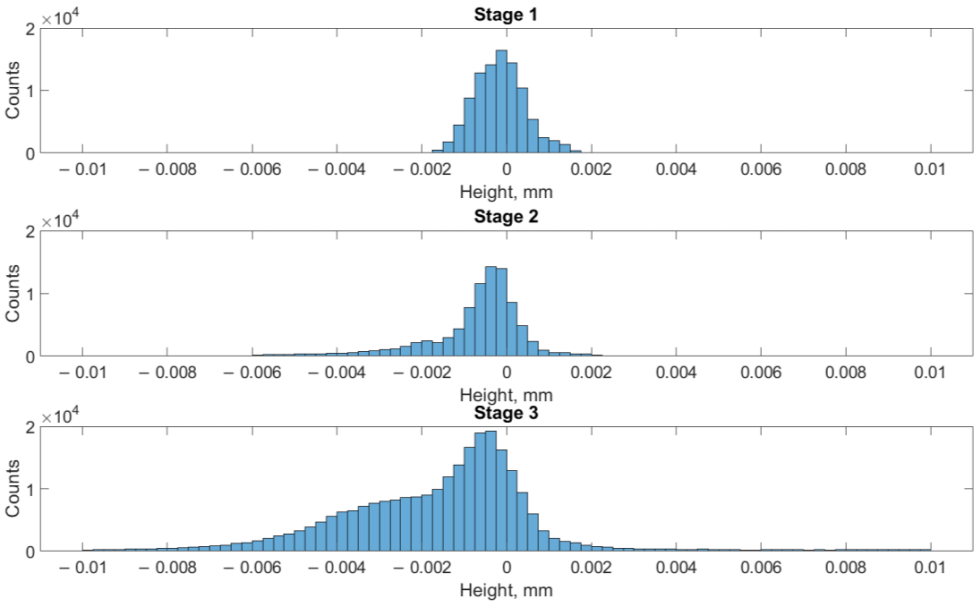

Figure 14. Distribution of series of peaks and troughs in the scratch after each stage of galling.

4. Discussion

The galling wear in this manuscript has been characterized and investigated via the evolution of the coefficient of friction, the lump growth on the tool and the scratch morphology.

4.1. Friction

The stochastic nature of galling has been observed in the friction curves (Figure 7), nevertheless the scratch test segments can be split into four categories. "Stage 1 only" is the stage when the coefficient of friction never rises above a certain threshold (0.32). Conversely, "stage 3 only" occurs when the coefficient of friction is above 0.9, very close to the start of the scratch test segment (e.g., refer to the galling stages summarized in Table 3). There are some scratch test segments that can be categorized as having all three phases of galling, and conversely again some tests that only have "stage 1" and "stage 2" phases, but no "stage 3" phase.

In accordance with the other literature [10,11], each successive stage of galling reaches a higher coefficient of friction, and so these data have been used to separate the three stages in the scratch morphology in this manuscript. It is reported in the literature that the rise in the coefficient of friction is due to the formation of an aluminum transfer layer, and that this stabilizes when a dynamic equilibrium is reached between the generation and ejection of loose wear particles [12]. However, the coefficient of friction reported in the tests in this current study generally monotonically increase during stage 2, rather than a constant intermediate friction coefficient as reported by Eriksson et al. [11]. Additionally, there was no "sharp rise" in coefficient of friction between stage 1 and stage 2, or between stage 2 and stage 3, which was also reported by Eriksson et al. [11] and Vilhena et al. [10].

As these experiments were conducted at room temperature, the strong adhesion Yang et al. [16] report (coefficient of friction reaching 1.5) is not seen. The maximum coefficient of friction observed in this work stabilized around a maximum of 1. However, as seen in the measurements of the scratch morphology (Section 3.3), the damage mechanisms and coefficient of friction measurements for the initial galling wear (stage 1) are similar to the observations by Yang et al. [16].

4.2. Lump Growth on the Indenter

Owing to the tribosystem being a closed system, the measurements can only be made post-test—hence only the transfer of material for the final stage observed can be investigated. That is, for the tests that are otherwise classified as showing two or three stages of galling, only the volume of transferred material in the final observed stage can be commented upon. Nevertheless, immediate transfer was seen in some tests (in agreement with other works), and later stages see more transferred material. Some studies report that adhered material can be moved, removed and abraded away, which is evidenced here as the increase in transferred volume between the stages is greatest for stage 2 to stage 3 (when considering the amount of material transferred). However, when considering the percentage increase, stage 1 to stage 2 see a far greater transfer of material than from stage 2 to stage 3.

It is widely reported that adhesion occurs on the harder of the two contacting surfaces [10,11,16,23–27], which has been seen in this work as shown by the lump growth on the steel indenter. Often, studies that have investigated the aluminum/steel tribopair, it is the tool/indenter that is made from an aluminum alloy and, as such, becomes abrasively worn by the harder steel sample plate [7,28,29]. Therefore, the galling behavior and lump growth for this configuration, where the tool/indenter is the harder material in the aluminum/steel tribopair, is understudied/under-reported.

4.3. Scratch Morphology

The results show that there is an obvious difference in the scratch morphology as the galling evolves. It is evident from Figure 12 that the evolution of the damage maybe characterized by the series of peaks and troughs running across the scratch.

The surface damage Yang et al. [16] reported is comparable to the damage seen in this work for the initial galling wear. However, as wear progresses, the results from Yang et al. [16] showed similar damage to that seen by Gaard et al. [30], with smaller scratches forming within the contact along the sliding direction. These previous studies attribute these longitudinal scratches to hard particles becoming trapped in the contact region. However, this behavior has not been observed in this current work.

In the literature it is reported that the scratch morphology is affected by adhesion and ploughing between surface asperities. Authors such as Gaard et al. [30] (working with steel-on-steel contacts) and Heinrichs et al. [31] (working with steel and aluminum alloys) state that the transferred material work hardens, or hardens by oxidation [13,23–26,32–37], in the contact region. Moreover, in some of the literature it is argued that the adhered material work hardens to an equal or greater hardness than that of the indenter, due to the work hardening of austenitic steels or the intrinsic hardness of aluminum oxides [4,13,38–40]. However, the damage observed in this current study suggests that these hardening processes do not occur in these tests—i.e., that there are no hard asperities being formed in the contact, during the material transfer from the Al5083 plate to the tool steel, or during the subsequent sliding. The tests were conducted at room temperature (indicative of cold forming) and low sliding speeds, which reduces the frictional heating. Therefore, it is possible that a lack of oxide formation may be playing a role here.

Despite this possibility, the effect of oxide formation is complex and it is unclear whether or not oxide formation will inhibit or accelerate galling wear. In some cases, oxide formation worsens the galling as it introduces hard particles into the contact; however, in other cases, the oxides themselves can reduce galling by acting as a barrier to metal-on-metal contact [7,10,18,39–41]. There is a consensus that metal-on-metal contact generates high levels of adhesion, typically more than metal–oxide contact. This further suggests that oxide layers have not been formed in the contacts in this current study, and the wear scenario has remained as a metal-on-metal contact.

Jue et al. [17,18] found that worn surfaces of 7075 aluminum alloy at different temperatures can be divided into two zones (a smooth zone and rough zone), and the relative areas of these zones varies with temperature. However, the reported smooth/rough zones are very close to one another, intermixed in some examples shown in the work [17,18]. The results presented in this manuscript do not have this mix of smooth and rough zones, rather there is a clear "smooth" zone that becomes a rough zone.

The scratch morphology, as measured by the optical profilometer, is shown in Figure 13, as a function of the height along the scratch length. To better observe the series of peaks and troughs in the scratch seen in the profile form measurement, a histogram of these (height) measurements is shown in Figure 14. In Figure 14 there is a clear change in the profile height distribution between each stage of galling wear. Each successive stage of galling results in a shift of the distribution further in the negative direction, with a corresponding shift in the distribution of material transferred to the indenter shifting to the positive direction, as shown in Figure 11. This indicates that, as the amount of material adhered to the indenter increased, the depth of the grooves on the scratch surface perpendicular to the sliding direction also increased. To the authors' best knowledge, there are no other studies on the distribution of damage within the wear scar. However, Moghadam et al. [42] report on the number of valleys deeper than 1 μm in relation to the drawing length of their tests.

5. Conclusions

The coefficient of friction between a tool steel and Al5083 during dry sliding at slow sliding speed and low loads, was measured and used to categorize the stages of galling wear, which were correlated to the lump growth and scratch morphology.

The following conclusions have been made:

- The galling evolution is characterized by the coefficient of friction regimes.
- Stage 1 showed little to no lump growth on the indenter. Stage 2 showed uniform lump growth, while stage 3 showed less uniform lump growth. In some cases, the lumps in stage 3 showed the development of a steep edge at the beginning of the lump.
- The scratch morphology from stage 2 and 3 showed a series of peaks and troughs across the scratch, as opposed to the expected damage mechanism of longitudinal scratches in the scratch.
- Using a novel investigation of the distribution of the heights of these peaks and troughs showed that, as the amount of material adhered to the indenter increased, the depth of the grooves on the scratch surface perpendicular to the sliding direction also increased.

Author Contributions: T.M.D.: conceptualization, experiments, data collection, formal analysis and draft writing, project administration. M.P.P.: conceptualization, experimental design, supervision, review and edit of writing, project administration. J.M.G.: supervision, review and proof reading. B.F.R.: supervision, review and proof reading. All authors have read and agreed to the published version of the manuscript.

Funding: This research received no external funding.

Data Availability Statement: The data presented in this study are available on request from the corresponding author. The data are not publicly available due to on-going research.

Acknowledgments: The authors would like to thank Alireza Vahid and Reza Parvizi for their technical support of the experimental regime and microscopy. We would also like to thank Matt Zampatti, Luke Tyrell and Robert Lovett for their technical support.

Conflicts of Interest: The authors declare no conflict of interest.

References

1. Shanbhag, V.V.; Rolfe, B.F.; Arunachalam, N.; Pereira, M.P. Investigating galling wear behaviour in sheet metal stamping using acoustic emissions. *Wear* **2018**, *414–415*, 31–42. [CrossRef]
2. Devenport, T.; Rolfe, B.; Pereira, M.; Griffin, J.M. Analysis of Acoustic Emissions for Determination of the Mechanical Effects of Scratch Tests. *Appl. Sci.* **2022**, *12*, 6724. [CrossRef]
3. Gåård, A.; Sarih, R. Influence of Tool Material and Surface Roughness on Galling Resistance in Sliding against Austenitic Stainless Steel. *Tribol. Lett.* **2012**, *46*, 179–185. [CrossRef]
4. Heinrichs, J.; Jacobson, S. Mechanisms of Transfer of Aluminium to PVD-Coated Forming Tools. *Tribol. Lett.* **2012**, *46*, 299–312. [CrossRef]
5. Shanbhag, V.V.; Rolfe, B.F.; Pereira, M.P. Investigation of Galling Wear Using Acoustic Emission Frequency Characteristics. *Lubricants* **2020**, *8*, 25. [CrossRef]
6. Hou, Y.; Yu, Z.; Li, S. Galling Failure Analysis in Sheet Metal Forming Process. *J. Shanghai Jiaotong Univ.* **2010**, *15*, 245–249. [CrossRef]
7. Pujante, J.; Pelcastre, L.; Vilaseca, M.; Casellas, D.; Prakash, B. Investigations into wear and galling mechanism of aluminium alloy-tool steel tribopair at different temperatures. *Wear* **2013**, *308*, 193–198. [CrossRef]
8. Daure, J.L.; Carrington, M.J.; McCartney, D.G.; Stewart, D.A.; Shipway, P.H. Measurement of friction in galling testing—An example of its use in characterising the galling behaviour of hardfacings at ambient and elevated temperature. *Wear* **2021**, *476*, 203736. [CrossRef]
9. Schedin, E. Galling mechanisms in sheet forming operations. *Wear* **1994**, *179*, 123. [CrossRef]
10. Vilhena, L.M.; Antunes, P.V.; Ramalho, A. Galling characterization for the pair composed by aluminium and M2 steel under dry and lubricated conditions by using load-scanning test method. *J. Braz. Soc. Mech. Sci. Eng.* **2018**, *40*, 284. [CrossRef]
11. Eriksson, J.; Olsson, M. Tribological testing of commercial CrN, (Ti,Al)N and CrC/C PVD coatings—Evaluation of galling and wear characteristics against different high strength steels. *Surf. Coat. Technol.* **2011**, *205*, 4045–4051. [CrossRef]
12. Liu, H.; Yang, X.; Zheng, Y.; Wang, L. Experimental Study on Galling Behavior in Aluminum stamping processes. *Phys. Sci. Forum* **2022**, *4*, 102022.
13. Gåård, A.; Krakhmalev, P.; Bergström, J. Wear Mechanisms in Galling: Cold Work Tool Materials Sliding against High-strength Carbon Steel Sheets. *Tribol. Lett.* **2009**, *33*, 45–53. [CrossRef]
14. Sindi, C.T.; Najafabadi, M.A.; Salehi, M. Investigation of surface damages during sheet metal forming using acoustic emission. *Proc. Inst. Mech. Eng. Part J J. Eng. Tribol.* **2013**, *227*, 286–296. [CrossRef]
15. Domitner, J.; Silvayeh, Z.; Shafiee Sabet, A.; Öksüz, K.I.; Pelcastre, L.; Hardell, J. Characterization of wear and friction between tool steel and aluminum alloys in sheet forming at room temperature. *J. Manuf. Process.* **2021**, *64*, 774–784. [CrossRef]

16. Yang, X.; Hu, Y.; Zhang, L.; Zheng, Y.; Politis, D.J.; Liu, X.; Wang, L. Experimental and modelling study of interaction between friction and galling under contact load change conditions. *Friction* **2022**, *10*, 454–472. [CrossRef]
17. Lu, J.; Song, Y.; Zhou, P.; Lin, J.; Dean, T.A.; Liu, P. Process parameters effect on high-temperature friction and galling characteristics of AA7075 sheets. *Mater. Manuf. Process.* **2021**, *36*, 967. [CrossRef]
18. Lu, J.; Song, Y.; Hua, L.; Zhou, P.; Xie, G. Effect of temperature on friction and galling behavior of 7075 aluminum alloy sheet based on ball-on-plate sliding test. *Tribol. Int.* **2019**, *140*, 105872. [CrossRef]
19. AISI 4140 Chrome-Molybdenum High Tensile Steel. Available online: https://www.azom.com/article.aspx?ArticleID=6116 (accessed on 30 May 2023).
20. Aluminium Alloys—Aluminium 5083 Properties, Fabrication and Applications. Available online: https://www.azom.com/article.aspx?ArticleID=2804 (accessed on 30 May 2023).
21. Pereira, M.P.; Yan, W.; Rolfe, B.F. Contact pressure evolution and its relation to wear in sheet metal forming. *Wear* **2008**, *265*, 1687–1699. [CrossRef]
22. Daure, J.L.; Kóti, D.; Carrington, M.J.; McCartney, D.G.; Stewart, D.A.; Shipway, P.H. Galling of stainless steels as a function of test conditions in an ASTM G196-type test setup—The role of temperature, rotational velocity, interrupted rotation and rotational distance. *Wear* **2023**, *524–525*, 204804. [CrossRef]
23. Safara Nosar, N.; Olsson, M. Influence of tool steel surface topography on adhesion and material transfer in stainless steel/tool steel sliding contact. *Wear* **2013**, *303*, 30–39. [CrossRef]
24. Budinski, K.G.; Budinski, S.T. Interpretation of Galling Tests. *Wear* **2015**, *332–333*, 1185–1192. [CrossRef]
25. Heinrichs, J.; Olsson, M.; Jacobson, S. Mechanisms of material transfer studied in situ in the SEM. *Wear* **2012**, *292–293*, 49–60. [CrossRef]
26. Heinrichs, J.; Olsson, M.; Jacobson, S. New understanding of the initiation of material transfer and transfer layer build-up in metal forming—In situ studies in the SEM. *Wear* **2012**, *292–293*, 61–73. [CrossRef]
27. Hu, Y.; Wang, L.; Politis, D.J.; Masen, M.A. Development of an interactive friction model for the prediction of lubricant breakdown behaviour during sliding wear. *Tribol. Int.* **2017**, *110*, 370–377. [CrossRef]
28. Vilaseca, M.; Molas, S.; Casellas, D. High temperature tribological behaviour of tool steels during sliding against aluminium. *Wear* **2011**, *272*, 105–109. [CrossRef]
29. Pujante, J.; Vilaseca, M.; Casellas, D.; Riera, M.D. The Role of Adhesive Forces and Mechanical Interaction on Material Transfer in Hot Forming of Aluminium. *Tribol. Lett.* **2015**, *59*, 10. [CrossRef]
30. Gåård, A.; Krakhmalev, P.; Bergström, J. Wear mechanisms in deep drawing of carbon steel—Correlation to laboratory testing. *Tribotest* **2008**, *14*, 1–9. [CrossRef]
31. Heinrichs, J.; Jacobson, S. Laboratory test simulation of galling in cold forming of aluminium. *Wear* **2009**, *267*, 2278–2286. [CrossRef]
32. Ghiotti, A.; Simonetto, E.; Bruschi, S. Influence of process parameters on tribological behaviour of AA7075 in hot stamping. *Wear* **2019**, *426–427*, 348–356. [CrossRef]
33. Choi, H.; Kim, S.; Seo, P.; Kim, B.; Cha, B.; Ko, D. Experimental investigation on galling performance of tool steel in stamping of UHSS sheets. *Int. J. Precis. Eng. Manuf.* **2014**, *15*, 1101–1107. [CrossRef]
34. Määttä, A.; Vuoristo, P.; Mäntylä, T. Friction and adhesion of stainless steel strip against tool steels in unlubricated sliding with high contact load. *Tribol. Int.* **2001**, *34*, 779–786. [CrossRef]
35. Gåård, A.; Krakhmalev, P.; Bergström, J. Influence of tool steel microstructure on origin of galling initiation and wear mechanisms under dry sliding against a carbon steel sheet. *Wear* **2009**, *267*, 387–393. [CrossRef]
36. Heinrichs, J.; Jacobson, S. The influence from shape and size of tool surface defects on the occurrence of galling in cold forming of aluminium. *Wear* **2011**, *271*, 2517–2524. [CrossRef]
37. Rogers, S.R.; Bowden, D.; Unnikrishnan, R.; Scenini, F.; Preuss, M.; Stewart, D.; Dini, D.; Dye, D. The interaction of galling and oxidation in 316L stainless steel. *Wear* **2020**, *450–451*, 203234. [CrossRef]
38. Karlsson, P.; Gåård, A.; Krakhmalev, P.; Bergström, J. Galling resistance and wear mechanisms for cold-work tool steels in lubricated sliding against high strength stainless steel sheets. *Wear* **2012**, *286–287*, 92–97. [CrossRef]
39. Mao, L.J.; He, X.; Cai, M.J.; Qian, L.Q. Influence of Contact Load on the Dry Sliding Wear Performance of 7075 Aluminum Alloy. *Exp. Tech.* **2023**, *47*, 357–367. [CrossRef]
40. Heinrichs, J.; Jacobson, S. Laboratory test simulation of aluminium cold forming—influence from PVD tool coatings on the tendency to galling. *Surf. Coat. Technol.* **2010**, *204*, 3606–3613. [CrossRef]
41. Huttunen-Saarivirta, E.; Kilpi, L.; Hakala, T.J.; Metsäjoki, J.; Ronkainen, H. Insights into the behaviour of tool steel-aluminium alloy tribopair at different temperatures. *Tribol. Int.* **2018**, *119*, 567. [CrossRef]
42. Moghadam, M.; Christiansen, P.; Bay, N. Detection of the Onset of Galling in Strip Reduction Testing Using Acoustic Emission. *Procedia Eng.* **2017**, *183*, 59–64. [CrossRef]